THE ASTROPHYSICAL JOURNAL, 304:657–663, 1986 May 15

LIMITS ON SUPERNOVA RATES AND INTERSTELLAR DENSITIES FROM X-RAY OBSERVATIONS OF M101

DONALD P. COX
Rice University and University of Wisconsin, Madison
AND
DAN MCCAMMON
University of Wisconsin, Madison
Received 1985 July 15; accepted 1985 November 11

ABSTRACT

Measurements of the X-ray surface brightness of a face-on disk galaxy M101 have previously been used to place upper limits on the power radiated by a hot corona. Such analysis constrains the effective density of the disk; either it must be so low that the remnants drive a fast hot wind (low radiated power) or so high that the remnant temperature at overlap is low (low X-ray power). These X-ray measurements are here used to constrain the properties of the population of supernova remnants evolving in the disk. This adds a further constraint since young remnants evolving in higher density radiate more of their energy in X-rays, whether or not they eventually overlap to generate a hot corona.

The strength of this second limit depends strongly on the density history of the remnants (e.g., evaporative vs. nonevaporative evolution) and on the assumed supernova rate. For evaporative evolution the analysis rules out the McKee and Ostriker interstellar medium (ISM) model in particular and evaporative evolution in general unless the supernova rate is at least several times lower than current expectations. For standard Sedov evolutions, the density limit marginally admits 0.2 cm^{-3}, a popular alternative to the McKee and Ostriker model.

Subject headings: galaxies: individual — nebulae: supernova remnants — X-rays: sources

I. INTRODUCTION

Two attempts to use the *Einstein* satellite IPC to measure the X-ray emission of fountains, coronae, or hot interstellar gas of noncluster disk galaxies have made no clear detection. Bregman and Glassgold (1982) studied two edge-on spirals (NGC 3628 and NGC 4244), a very sensitive test for coronae and fountains, while McCammon and Sanders (1984) tried the face-on spiral M101, for which X-ray–emitting material dispersed through the interstellar medium could potentially be seen. In both cases it was found that the upper limits on the X-ray emission were some two orders of magnitude lower than the supernova power estimated to be available. Essentially the same conclusion applies to a local region of our own Galaxy where the measured surface brightness of the soft X-ray background is a similarly small fraction of the mean surface density of supernova power (e.g., Cox 1981, 1983).

These results restrict the manner in which supernova energy is dissipated, thus limiting the range of tenable models for supernova remnant evolution in the interstellar medium. At a given supernova rate, the model parameter most directly constrained is the degree to which remnants, on average, dilute their energy with interstellar material before overlapping one another or entering the radiative phase.

The options available prior to these restrictions seem to have been:

1) Little dilution (less than $\sim 100\ M_\odot$ per supernova, very low density ISM, and little evaporation); SN energy drives a hot, low-density wind from the galaxy. Owing to the low density, X-ray emission is weak.

2) Intermediate dilution (a few hundred solar masses per supernova); SN generate an active fountain or halo which radiates the entire SN power in X-rays and EUV. The fraction of the power radiated in X-rays decreases with increasing dilution (more mass dilution implies lower coronal temperature).

3) Critical dilution ($\sim 3000\ M_\odot$ per SN, acquired late at low effective density); individual remnants radiate the bulk of their energies shortly before overlap with one another, providing a large filling fraction of hot gas in the disk. The coronal component temperature is so low that it emits few X-rays. This is the general form of the McKee and Ostriker model (1977; hereafter MO). Or finally,

4) Large dilution (high-density ISM or much evaporation) individual remnants become radiative while still relatively small, forming large expanding shells that snowplow through the medium until encountering one another long after the transition to the radiative phase.

One might suppose that for dilution even greater than the critical value, X-ray detectors would be insensitive probes. For observations of a face-on spiral galaxy, however, such is not the case. A detector can look into the disk and record the integrated surface brightness of the population of *individual* remnants. Even at critical dilution, X-ray emission by young hotter remnants can be significant. For greater ISM density or higher thermal evaporation from clouds (either case providing greater density of hot material within remnants and greater dilution), the X-ray emission of the individual remnants in the population is higher.

For a given supernova rate, the X-ray surface brightness can thus be used to set limits on both coronal and remnant population properties, the former constraining the intermediate dilution possibilities (setting a lower limit on dilution in that regime), the latter constraining higher dilutions and setting an upper limit. For an important subset of possibilities (the

assumption of evaporative remnants), these two limits on M101 turn out to be mutually exclusive, implying either that the supernova rate is lower than expected or hot remnants evolve in a less X-ray–emissive fashion.

The average galactic distribution of emission measure (vs. temperature) from its population of individual remnants is calculated in § II. Section III reviews the analysis of the *Einstein* IPC measurements of M101 by McCammon and Sanders (1984) and presents the upper limit on the remnant population properties. The latter is derived by restricting the calculated X-ray brightness, from the emission-measure distribution of § II, to be less than the observational limit. The surface brightness depends on four parameters (supernova power, characteristic remnant density in the X-ray–emitting regime, density evolution of remnants with age, and overburden of X-ray–absorbing material in M101). For reasonable estimates of the supernova power and absorption, the limit is expressed as a maximum remnant internal density in the X-ray–emitting regime (specifically at 10^6 K), as a function of the assumed mode of remnant evolution.

For remnant evolution with constant or increasing average density, the extreme upper limits on remnant internal densities are comparable to the average interstellar density in the Milky Way, certainly exceeding the expected density within large supernova remnants. For some reasonable parameter choices, however, the constant average density case marginally threatens to exclude an important possibility. For evaporative remnants, whose mean internal density decreases with radius, the density limit is more stringent. The broader implications of the latter are considered in § IV, which studies both the remnant population and coronal emission limits, deriving the properties of an MO state which is just barely consistent with the X-ray limit. The results are summarized in Figure 2. Section V presents an overview of the results and discusses the importance of future observations on studies of this type.

II. THE EMISSION-MEASURE DISTRIBUTION OF A POPULATION OF REMNANTS

Although an isolated supernova remnant may radiate the bulk of its energy only after evolving to a rather low temperature ($<4 \times 10^5$ K), it nevertheless passes through a phase at X-ray–emitting temperatures and radiates some of its energy there. As a result, a steady state population of such remnants will always have some members contributing to a high-temperature tail of the emission-measure distribution function.

For this study we will assume that individual remnants mature in an isotropic environment and radiate as though they were completely in collisional equilibrium at the postshock temperature. The effect of this assumption can be assessed from the results of Cox and Anderson (1982) and Hamilton, Sarazin, and Chevalier (1983). Using the equilibrium rates slightly underestimates the X-ray emissivity. Assuming that the emission spectra can be represented by the postshock temperature will ignore emission from the hot interiors of remnants which have slowed too much to generate X-rays at the edge. More detailed calculations would therefore provide more restrictive upper limits on the high-temperature tail of the emission measure distribution and the effective density of X-ray–emitting remnants.

The hot mass within a supernova remnant during the adiabatic phase will be proportional to radius cubed only in the simplest case. Generalizing to

$$M \propto R_s^{3+b} , \tag{1}$$

where $b = -5/3$ is the MO thermal conduction value, $b = 0$ for a homogeneous medium, and b is positive for evolution in a cavity where density increases gradually with radius, we then have

$$T_s \propto v_s^2 \propto E_0/M , \quad R_s \propto t^{2/(5+b)} , \quad \text{and} \quad v_s = [2/(5+b)]R_s/t .$$

It is straightforward to express all of the evolving parameters of a remnant as power laws of the postshock temperature. An important example is the distribution of remnant ages over temperature:

$$\frac{dt}{dT} = -\frac{5+b}{2(3+b)}\frac{t}{T} . \tag{2}$$

The luminosity of a single remnant can be written (e.g., Cox 1986*a*)

$$\mathscr{L} = \beta(b, q) N n_A L(T_s)$$

or

$$\mathscr{L} = \beta'(b, q)\bar{n}^2 V L(T_s) \tag{3}$$

where V is the remnant volume, $N = 3Vn_A/(3+b)$, n_A is the effective preshock ambient density (the actual value except in evaporative models), $\bar{n} = 3n_A/(3+b)$ is the average density of hot gas within the remnant, the parameter q arises from the assumption that the cooling function $L(T)$ is proportional to T^{-q}, and β and $\beta' = (3+b)\beta/3$ are effective compaction parameters (see Cox and Franco 1981 or Cox 1986*a* for examples). Dividing $\mathscr{L}$ by $L(T_s)$ provides the effective value of $\int n_e^2\, dV$ at T_s.

In a disk galaxy of area A_g and supernova rate $(\tau_{SN})^{-1}$, the number of remnants in the postshock temperature range T to $T + dT$ per unit area of the disk is

$$dv = \frac{1}{A_g \tau_{SN}}\left|\frac{dt}{dT}\right| dT , \tag{4}$$

so that the distribution function over temperature of surface averaged emission measure is

$$\frac{d(\mathrm{EM})}{dT} = \frac{\mathscr{L}(T)}{L(T)}\frac{1}{A_g\tau_{SN}}\frac{5+b}{2(3+b)}\frac{t}{T}$$

$$= \frac{3(5+b)\beta}{2(3+b)^2}\frac{n_A^2(T)}{A_g\tau_{SN}}\frac{V(T)t(T)}{T} . \tag{5}$$

Choosing a particular temperature T_0 at which to normalize these results, they can be written entirely as functions of conditions when $T_s = T_0$ (all shown with subscript zero), multiplied by a power law in T_s/T_0:

$$\frac{d(\mathrm{EM})}{d(T/T_0)} = \frac{1}{A_g\tau_{SN}}\left[\frac{3(5+b)\beta}{2(3+b)^2} V_0 n_{A0}^2 t_0\right]\left(\frac{T_0}{T_s}\right)^{[17+7b)/[2(3+b)]} . \tag{6}$$

By using the numerical integrals in Cox and Franco 1981 (see also Cox 1986*a*) the square bracket for $b \geq 0$ can be approximated

$$\frac{3(5+b)\beta}{2(3+b)^2} V_0 n_{A0}^2 t_0 \approx 1.2 \times 10^{72}\ \mathrm{cm}^{-3}\mathrm{s}\ G(b)\ E_{51}^{4/3}\ \bar{n}_0^{2/3} \times (10^6\ \mathrm{K}/T_0)^{11/6} , \tag{7}$$

where

$$G(b) = \frac{19}{36}\beta\frac{1}{(1+0.239b)^{4/3}} , \tag{8}$$

defined such that $G(0) = 1$. The function $\beta(b, q)$ was evaluated for $q = -\frac{1}{2}$ by Cox (1986*a*) from the Cox and Franco (1981) integrals to be (for positive b):

$$\beta = \frac{3}{3+b}\beta' \approx \frac{12(3+b)}{19+8b}. \quad (9)$$

For $b = -5/3$, the evaporative case, $\beta' = 2$ (implying $\beta = 4.5$) was advocated by Cox (1986*a*) because the above formula from fitting positive b results suggests an absurdly small compaction parameter at $b = -5/3$. Choosing the normalization to be $T_0 = 10^6$ K to place it in the X-ray regime, and expressing the supernova rate per unit area relative to 1 SN per 30 years within a disk of radius 15 kpc, we finally have

$$\frac{d(\mathrm{EM})}{d(T/10^6\ \mathrm{K})} = (6.3 \times 10^{-2}\ \mathrm{cm}^{-6}\ \mathrm{pc})G(b)\left(\frac{10^6\ \mathrm{K}}{T}\right)^{(17+7b)/[2(3+b)]} \times \left(\frac{15\ \mathrm{kpc}}{R_g}\right)^2\left(\frac{30\ \mathrm{yr}}{\tau_{\mathrm{SN}}}\right)E_{51}^{4/3}\,\bar{n}_0^{2/3}. \quad (10)$$

For fixed $\bar{n}_0$, this distribution weights high temperatures more heavily for negative values of b because the remnants are then denser when hot. Notice that n_{A0} is specifically the effective preshock density when the postshock temperature is 10^6 K, while $\bar{n}_0$ is the average density within the remnants at that temperature. Depending on b, the densities can be either higher or lower at earlier epochs. A population of remnants with a distribution function for $\bar{n}_0$ simply introduces $\langle \bar{n}_0^{2/3} \rangle$, while a distribution of b values would be more complicated.

An important caveat regarding the above approximation is that remnants have been assumed to be evolving in an isotropic environment so that their luminosities and radial evolution are coupled via $n_A(R_s)$. The inclusion of significant inhomogeneity in the density distribution on a scale comparable to the remnant size, like that observed, for example, in the Cygnus Loop, complicates the analysis considerably, making the density values inferred in this study measures of something intermediate between the most pervasive density and the density of the brightest X-ray–emitting features. Such inhomogeneities can be regarded as enhancing the effective value of the compaction parameter β'. Since this parameter provides the conversion between rms and average density, using the value appropriate to isotropic remnants is conservative in evaluating the upper limit to the average density within remnants.

III. COMPARISON WITH M101

The *Einstein* satellite IPC measurements of M101 were analyzed by McCammon and Sanders (1984; hereafter McS) in concentric rings of outer radius $5i'$, where $i = 1, 5$. The visible galaxy is prominent in rings 1 and 2. The three historical supernovae occurred in rings 2 and 3. The Holmberg radius lies approximately at the outer boundary of ring 3. Data in the vicinity of identifiable sources were omitted.

The results of these observations were that:

1) Rings 2–5 have essentially identical soft X-ray surface brightness, all slightly *lower* than anticipated from the rocket measurements of the 8° average soft X-ray background in that direction. The background is unusually bright in this region, but there is no indication that it requires other than the usual origin in the solar vicinity. The surface average emission measure of M101 hot gas in these outer rings is certainly less than that of the Local Bubble.

2) Ring 1 has a detectable excess count rate but, comparing IPC exposures separated by six months, some of the soft X-ray flux is clearly varying in time. It is not known how much of the remaining ring 1 flux should be attributed to non–SNR sources.

The observed count rates and their 1 σ uncertainties are in Table 1. By considering rings 4 and 5 as background (non–X-ray plus foreground emission) measurements, upper limits can be set on the SNR–induced count rate for rings 1–3. Roughly speaking (depending on channel), the 3 σ limits are then 80%, 10%, and 10%, respectively, of the total observed rates in rings 2–5.

The emission measure distribution in equation (10), combined with Raymond and Smith (1977, 1979) equilibrium spectra and absorption due to assumed intervening material, is folded through the IPC response function to calculate anticipated count rates in each IPC channel. This must be done separately for each interesting value of b (choice of SN evolution mode) and N_{H} (assumed column density of absorbing material). The calculation performed was normalized to

$$B \equiv \left(\frac{15\ \mathrm{kpc}}{R_g}\right)^2\left(\frac{30\ \mathrm{yr}}{\tau_{\mathrm{SN}}}\right)E_{51}^{4/3}\,\bar{n}_0^{2/3}. \quad (11)$$

Notice that B is proportional to the supernova power per unit area multiplied by the cube root of the Chevalier scaling parameter En^2. The integral over the temperature distribution of equation (10) can be extended to $T = 0$ because remnant cooling, at densities of interest, does not set in to alter or truncate the distribution until shock temperatures below those to which the IPC is sensitive.

By weighting the channels of greater count rate more heavily and imposing overall consistency at the 3 σ level with the set of rates and their standard deviations, one finds the 3 σ upper limit to the normalization parameter B. Two cases were considered: ring 1 alone (minus the average background of rings 4 and 5) and an area weighted average of rings 2 and 3 (again, minus 4, 5). The results are shown in Figure 1 where the hydrogen column density is in units of 10^{20} cm^{-2} and the indicated value is in addition to the 1.1×10^{20} cm^{-2} contribution of the Milky Way in the M101 direction. As expected from equation (10), the limit on B is tighter for smaller b. In addition, the limit on B for rings 2 and 3 is consistently a factor of ~ 9 more stringent than for ring 1, scaling with the respective X-ray limits. Owing to the unknown contribution from nondiffuse sources, ring 1 will not be considered further.

If remnants evolve in very low densities so that they achieve large sizes, then a small N_{H} overburden is expected, at least for the near side. (Our Local Bubble has $\sim 1.2 \times 10^{20}$ cm^{-2}.) Conversely, remnants evolving in higher density remain small

TABLE 1

EINSTEIN IPC OBSERVATIONS OF M101[a]

	Concentric Ring Number of Width 5′					
Channel	1	2	3	4	5	6
2.....	11.9 (3.5)	10.2 (1.1)	10.5 (0.7)	12.6 (1.0)	10.7 (1.7)	8.5 (1.1)
3.....	11.8 (3.2)	9.8 (0.9)	9.4 (0.6)	9.1 (0.7)	8.6 (1.5)	8.8 (0.9)
4.....	11.3 (2.7)	6.8 (0.7)	6.6 (0.5)	6.7 (0.6)	7.1 (1.2)	5.7 (0.7)
5.....	8.1 (2.5)	5.3 (0.7)	3.6 (0.4)	5.1 (0.5)	6.3 (1.1)	4.9 (0.6)
6.....	3.9 (2.1)	4.2 (0.6)	3.2 (0.4)	3.2 (0.5)	3.0 (0.9)	3.0 (0.6)
7.....	5.9 (2.2)	2.3 (0.5)	2.0 (0.4)	2.0 (0.4)	1.4 (0.8)	2.6 (0.6)

[a] Rates in units of 10^{-5} counts (arcmin^2 s)$^{-1}$ are followed in brackets by their 1 σ uncertainties.

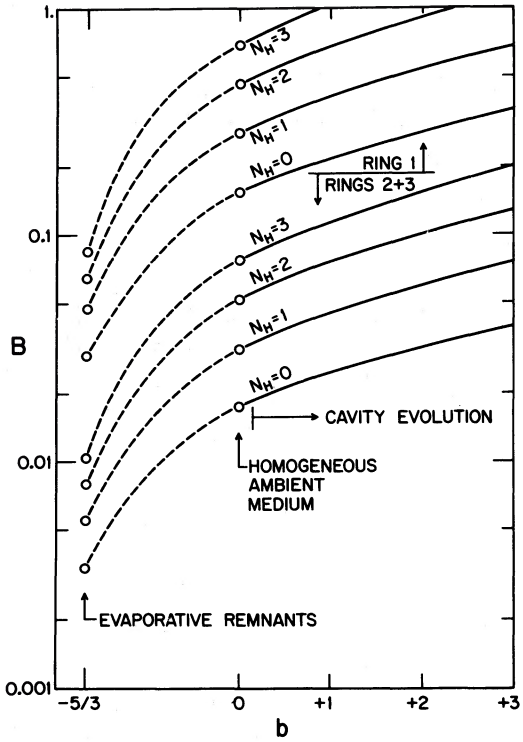

FIG. 1.—Upper Limits to the brightness factor B. The limits are shown vs. the density evolution factor b for various values of the hydrogen column density N_H (in units of 10^{20} cm^{-2}) assumed to overlie the emitting material in M101. Upper four curves are for ring 1 (minus 4 + 5 as background), the lower four are for rings 2 + 3.

and more likely to experience half of the 6×10^{20} cm^{-2} full disk column density characteristic of M101 as a whole.

Figure 1 should serve as a constant reminder of the tenuous nature of the conclusions about to be presented. Continuing in a conservative vein, we discuss only the upper limit provided by the $N_H = 3 \times 10^{20}$ cm^{-2} results.

From Figure 1 we infer that for evaporative evolution, $B < 0.01$; for evolution at constant average density, $B < 0.08$; while for evolution with mean density increasing as radius cubed, $B < 0.2$. Writing the normalized supernova power per unit area

$$P = E_{51}\left(\frac{15 \text{ kpc}}{R_g}\right)^2\left(\frac{30 \text{ yr}}{\tau_{SN}}\right), \quad (12)$$

such that

$$B = P(E_{51}\bar{n}_0^2)^{1/3}, \quad (13)$$

we can then write the effective remnant density at the epoch $T_s = 10^6$ K:

$$\bar{n}_0' \equiv \langle \bar{n}_0^{2/3} \rangle^{3/2} = (B/P)^{3/2}/E_{51}^{1/2}. \quad (14)$$

Uncertainty in the supernova explosion energy introduces at least a factor of 4 uncertainty in density limits. Once again taking the conservative position with $E_{51} \geq 0.5$, $\tau_{SN} \leq 100$ yr per 15 kpc radius area, we have $P \geq 0.15$, and

$$\bar{n}_0' \lesssim 24B^{3/2}. \quad (15a)$$

For $b = -5/3$, 0, and 3 the extreme upper limits on $\bar{n}_0'$ are then 0.03, 0.6, and 2 cm^{-3}, respectively. Unless the supernova rate is especially low, these are the maximum allowable average densities of hot gas within remnants whose shock temperature is 10^6 K.

From a study of this type one is interested in learning whether remnants might conceivably evolve in an intercloud medium of density 0.1–0.3 cm^{-3} or whether they necessarily evolve in a much lower density component, with or without appreciable thermal evaporation of embedded clouds. For $b \geq 0$, it is clear that limits posed by the *Einstein* observations are too weak to disallow any interesting possibility for $E_{51} = 0.5$ and $P = 0.15$. In fact, the $b = 0$ standard Sedov case has the more general result

$$\bar{n}_0' < \frac{0.023 \text{ cm}^{-3}}{E_{51}^2}\left(\frac{R_g}{15 \text{ kpc}}\right)^3\left(\frac{\tau_{SN}}{30 \text{ yr}}\right)^{3/2} (b = 0), \quad (15b)$$

so that insistence on $E_{51} = 1$ and contributing supernova rate per unit area comparable to that in the Milky Way *does* endanger the possibility of a moderate-density intercloud component. With improved observations discussed in § V, a definitive statement may be possible. In the meantime, the limit for the evaporative case is already so strong that only low-density remnants are compatible. The limits from individual remnants and hot coronae are combined in the next section, showing the severity of the problem with this mode.

IV. EVAPORATIVE EVOLUTION

The X-ray surface brightness of a galactic disk whose supernova remnants undergo evaporative evolution depends on three parameters: the supernova power per unit area (P), the effective density of remnants at some fiducial temperature ($\bar{n}_0$), and the column density of absorbing material. Having taken half the total column density as representative of the latter, we now pursue the regime in P, $\bar{n}_0$ space allowed by $B < 10^{-2}$. In addition to criteria separating allowed from disallowed regions, we shall present those distinguishing intermediate from high dilution regimes. The plane and its subdivisions are represented in Figure 2.

Approximate remnant properties as functions of E_0, b, T_s, and $\bar{n}$ were presented in Cox (1986*a*). For $b = -5/3$, the needed results include the extrapolated adiabatic phase temperature at the cooling epoch:

$$T_c = 0.88 \times 10^6 \text{ K}(E_{51}\bar{n}_c^2)^{1/7} = 0.82 \times 10^6 \text{ K}(E_{51}\bar{n}_0^2)^{2/9}, \quad (16a)$$

and the corresponding radiated fraction of the original energy

$$f_c = 0.68, \quad (16b)$$

where $\bar{n}_c$ is the average remnant density at that epoch. The general relation between density and temperature is

$$\bar{n} = \bar{n}_0 \bar{T}_6^{5/4} = \bar{n}_c(T_6/T_{6,c})^{5/4}.$$

The remnant radius as a function of $\bar{n}$ and $T_6 = T_s/10^6$ K is

$$R_s = 22.8 \text{ pc}\left(\frac{E_{51}}{\bar{n}T_6}\right)^{1/3}, \quad (17)$$

while the areal porosity factor is

$$Q_A \equiv \int_0^t \frac{\pi R_s^2 dt}{(\pi R_g^2 \tau_{SN})} = 1.75 \times 10^{-3}\frac{P}{\bar{n}T_6^{3/2}}. \quad (18)$$

The latter is related to the radiated fraction by

$$Q_A = Q_{A,c}(f/0.68)^{11/6}. \quad (19)$$

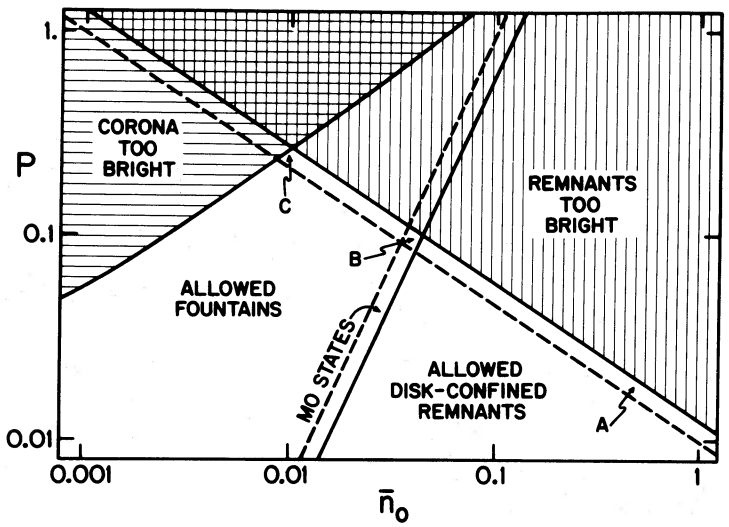

FIG. 2.—Constraints on populations of evaporative remnants in M101 for $B < 0.01$. The quantity P is the normalized supernova power per unit area of eq. (12), while $\bar{n}_0$ is the average density of the hot component within a remnant when the temperature is 10^6 K. Solid lines are for $E_{51} = 0.5$, while dashed are for $E_{51} = 1$. Locus A is from eq. (13). Intersection B is from eq. (26). (The remnant properties for conditions at this intersection are provided by eq. [32].) Intersection C is from eq. (31). The boundary to acceptable fountains follows from combining eqs. (13), (29), and (30b). The MO state locus, from eq. (23), separates the intermediate dilution regime of fountains and radiative coronae from the high-dilution regime of disk-confined remnants.

We continue the notation using B and P of equations (11) and (12).

The parameters of a population that behaved approximately in accordance with the McKee and Ostriker (1977) ISM model (critical dilution) can be inferred by forcing Q_A to be $\frac{1}{2}$ at the cooling epoch. They include: the average density, temperature, and radius at that epoch:

$$\bar{n}_c = \frac{0.022 \text{ cm}^{-3}}{E_{51}^{3/20}} \left(\frac{P}{2Q_{A,c}}\right)^{7/10}, \tag{20}$$

$$T_{6,c} = 0.29 E_{51}^{1/10} \left(\frac{P}{2Q_{A,c}}\right)^{1/5}, \tag{21}$$

$$R_{s,c} = 123 \text{ pc } E_{51}^{7/20} \left(\frac{2Q_{A,c}}{P}\right)^{3/10}; \tag{22}$$

the average density and radius at 10^6 K:

$$\bar{n}_0 = \frac{0.10 \text{ cm}^{-3}}{E_{51}^{11/40}} \left(\frac{P}{2Q_{A,c}}\right)^{9/20}, \tag{23}$$

$$R_{s0} = 49 \text{ pc } E_{51}^{17/40} \left(\frac{2Q_{A,c}}{P}\right)^{3/20}; \tag{24}$$

and the brightness factor for the population

$$B = 0.22 \frac{E_{51}^{3/20} P^{13/10}}{(2Q_{A,c})^{3/10}}. \tag{25}$$

In Figure 2, the locus of MO states is provided by equation (23) with $Q_{A,c} = 0.5$.

Although the densities, temperatures, and radii seem quite reasonable for $P \approx 1$, it is clear that the X-ray emission would in that case be far greater than the upper limit for M101. It is in this sense that the X-ray limit is restrictive of the critical dilution possibilities. Consistency is possible only if the supernova rate is small.

The MO state providing a brightness factor B requires

$$PE_{51}^{3/26} = 0.09(100B)^{10/13} \tag{26}$$

and

$$\tau_{SN} = 330 \text{ yr } E_{51}^{29/26} \left(\frac{15 \text{ kpc}}{R_g}\right)^2 \frac{1}{(100B)^{10/13}}. \tag{27}$$

Thus, since $100B < 1$, our upper limit on the X-ray emission of this MO state population is consistent only with a supernova rate per unit area 4–11 times smaller (depending on E_{51}) than that commonly assumed for the Milky Way. In Figure 2, intersection B is provided by equation (26) with $100B = 1$.

The evaporative remnant scenario is not tied directly to the MO condition that cooling occur slightly before overlap. That condition is specific to the choice of cloud population and supernova rate used. (MO argue that the cloud population will adjust to bring this about, but let us suppose that it does not.) More generally, then, the X-ray consistent conditions are

$$\bar{n} = \frac{10^{-3} \text{ cm}^{-3}}{E_{51}^{1/2}} \left(\frac{100B}{P}\right)^{3/2} T_6^{5/4}, \tag{28a}$$

$$R_s = 228 \text{ pc} \left(\frac{E_{51}P}{100B}\right)^{1/2} \frac{1}{T_6^{3/4}}, \tag{28b}$$

$$T_6 = 1.23 \left(\frac{E_{51}P^5}{Q_A^2(100B)^3}\right)^{2/11}. \tag{28c}$$

In Figure 2, locus A is provided by equation (28a) with $T_6 = 1$, or equation (13), and $100B = 1$. It provides the $n_0(P)$ limit between allowed and overly bright remnant populations. The formal value of the areal filling factor at the cooling epoch is

$$Q_{A,c} = 1.43 \times 10^4 \frac{E_{51}^{1/2} P^{13/3}}{(100B)^{10/3}}. \tag{28d}$$

Low and intermediate dilutions accompany $Q_{A,c} > 0.5$, and high dilution accompanies $Q_{A,c} < 0.5$. If the M101 remnants follow an evaporative evolution yet provide $B \leq 10^{-2}$, then unless P is small, remnants will overlap long before cooling. Very low densities and large radii are then the rule, in addition to remnant merger to form a hot corona.

These conditions have been made already consistent with the X-ray brightness, so the results seem to ascribe a maximum value of n_0 consistent with P, *for any value of* P. If however, remnant overlap occurs while the temperature is still in the X-ray–emitting regime ($T \geq 5 \times 10^5$ K), the corona is also subject to the constraints of the McS analysis. As we shall see, these evaporative evolutions leading to a hot corona are also too bright in X-rays, again, unless the supernova power is less than normal.

The conditions at the base of a galactic fountain or wind are like those of the source remnants when $Q_A \approx \frac{1}{3}$ (Cox 1986*b*). Thus the fountain temperature can be expected from equation (28c) to be approximately

$$T_{6,f} \approx 1.23\left(\frac{9E_{51}P^5}{(100B)^3}\right)^{2/11} . \quad (29)$$

The McS surface brightness limits were given for 2 σ confidence, so even though we are now considering halo emission we adopt their $N_{\rm H} = 2 \times 10^{20}$ cm^{-2} results to remain conservative. For $T_f < 10^6$ K their surface brightness limit can be approximated by

$$S < 10^{-(8.55-1.5/T_{6,f})} \text{ ergs cm}^{-2} \text{ s}^{-1} \text{ sr}^{-1} , \quad (30a)$$

which corresponds to

$$P < 10^{-(3.66-1.5/T_{6,f})} . \quad (30b)$$

The behavior of the exponential is sufficiently strong that unless E_{51}, or $100B$ is very different from 1, consistency with equation (29) requires $T_{6,f} < 0.50$, and

$$PE_{51}^{1/5} < 0.24(100B)^{3/5} . \quad (31)$$

The more precise criterion is shown in Figure 2 as the boundary between the allowed fountain and overly bright coronal regimes. The presence of B in equation (31) may seem extraneous, since we have imposed the McS analysis. The X-ray result has in fact been used twice. The evolving remnants must not generate too many X-rays before overlap (introducing B) nor must the resulting fountain after overlap. It is represented in Figure 2 by intersection C.

Consulting the now complete Figure 2 we find the highest allowed supernova power to be at intersection C in the intermediate dilution regime. Its numerical value is given by equation (31). Similarly, the highest power allowed to an MO state (critical dilution) is at intersection B, the numerical value provided by equation (26). High dilution possibilities have essentially this same upper limit to their power. Remnant density $\bar{n}_0 \approx 0.1$ can be accommodated by a further reduction in power by a factor of 2 to $P \approx 0.05$. Finally, low dilutions, leading to coronal temperatures in excess of 2×10^6 K and hot winds with little X-ray emission, are still conceivable, but they lie off the upper left corner of Figure 2. Their exact delineation is outside the scope of this paper.

Allowing a supernova rate which just barely prevents an X-ray–luminous corona (as at intersection C in Fig. 2) is a dangerous game. Owing to the temperature sensitivity of the emission, very small irregularities in local supernova rates, or cloud populations for evaporation, could lead to local hot spots in the fountain that would violate the constraint. The MO state is thus a better bet as an upper limit on the rate.

For this reason, and because it offers a specific standard for comparison, we finally present the parameters of the MO state which is just barely consistent with the present limit. It falls to future studies of the M101 remnant population to discover whether these results are an accurate portrayal. The parameters are

$$\tau_{\rm SN} R_g^2 = 330 \text{ yr}(15 \text{ kpc})^2 E_{51}^{29/26} , \quad (32a)$$

$$R_s = 70 \text{ pc } E_{51}^{23/52}/T_6^{3/4} , \quad (32b)$$

$$\bar{n} = 0.035 \text{ cm}^{-3} T_6^{5/4}/E_{51}^{17/52} , \quad (32c)$$

$$t = 1.52 \times 10^5 \text{ yr } E_{51}^{23/52}/T_6^{5/4} , \quad (32d)$$

$$\mathscr{L} = 1.34 \times 10^{37} \text{ ergs s}^{-1} E_{51}^{35/52}/T_6^{1/4} , \quad (32e)$$

$$f = 0.053 E_{51}^{3/26}/T_6^{3/2} , \quad (32f)$$

$$Q_A = 0.0046 E_{51}^{11/52}/T_6^{11/4} = 1.01 f^{11/6} . \quad (32g)$$

In this list, R_s, $\bar{n}$, t, $\mathscr{L}$, and f are the shock radius, mean remnant density (hot phase only), age, luminosity, and radiated fraction of the total energy, as functions of the postshock temperature. The quantity Q_A is the areal filling factor of the disk for remnants with postshock temperatures T and higher. Notice that the required supernova rate, at least that in the disk but outside superbubbles, is quite low, as are the remnant densities. Conditions at the cooling and merger epoch can be found from setting $Q_A = 0.5$.

V. OVERVIEW

Given the propriety of the general model of § II, the remaining assumptions acted to maximize the upper limit on the brightness parameter B. For the standard Sedov solution ($b = 0$), the resulting limit on density within remnants is given by equation (15b). At the expected supernova rate, it marginally threatens the possibility that remnants evolve in an intercloud component of density 0.1–0.3 cm^{-3}.

For evaporative evolution of remnants, no consistent system exists at the expected supernova rate. The possibilities at lower power are summarized in Figure 2. Below normalized supernova power per unit area (eq. [12]) $P \approx 0.2$, a broad range of possibilities opens up. The critical dilution MO states and high dilution disk confinement of remnants are available for $P < 0.09$.

Any further conclusions depend sensitively on one's disposition. If one favors MO states, one might be led to believe $E_{51} \lesssim 0.5$, particularly after remnants have suffered cloud compression and cosmic-ray acceleration losses. One is then driven to accept a low rate ($\tau_{\rm SN} > 150$ yr per disk area of radius 15 kpc) for relevant supernova—or to faultfinding with the assumptions of § II. Conversely, one might be tempted to see yet another nail in the coffin of MO ISM models. Pushing then for return to a higher density intercloud component, one finds that the then maximum acceptable SN rate for $b = 0$ is only a factor of 3 above that which admits the MO state for $b = -5/3$. Perhaps that is comfortable but one must keep a wary eye on the conservative assumptions leading to the limit, as well as future observations and refined analysis that will almost certainly push it downward. Those familiar with the disquieting X-ray properties of the LMC remnant population (e.g., Long 1983; Cox 1986*a*) may just be further convinced that the remnants do not evolve as expected and that this type of study must wait until individual remnants in the population can be studied. Finally, one might see further confirmation of the need to consider correlated SN explosions in clusters as an important component, possibly driving a hot nonradiative wind, reducing the residual SN rate with which the general disk must cope.

While some useful constraints are placed by the *Einstein* observations, other potential conclusions are statistically marginal or just out of reach, and data of even this quality do not exist for any suitable galaxy except M101. The observational situation should improve tremendously in the foreseeable future, however. The Advanced X-Ray Astrophysics Facility (AXAF) will of course have greatly improved angular resolution and sensitivity, but on a shorter time scale Germany's Röntgen Satellite (ROSAT) should be very well matched to this particular task. Its 2 keV upper energy cutoff is no disadvantage, and optimization for lower energies provides a net effective area almost 5 times that of *Einstein* at 280 eV (and almost half that of AXAF). A much more important consideration is that at 20″ half-power radius, the IPC angular resolution is a factor of 3 better than *Einstein*. This allows far more effective removal of point-source contributions and permits observations of more distant galaxies, thus greatly increasing the sample size.

The faster optics and improved IPC should result in an extraneous detector background which is usually quite negligible compared to the diffuse X-rays. This and the more stable and linear operation of the new IPC will greatly reduce the systematic uncertainties which complicate analysis of diffuse data from *Einstein*. Another major benefit will be improved energy resolution which permits unambiguous separation of the 0.100–0.280 keV X-rays from those in the 0.500–1.00 keV band. This will allow some useful temperature limits to be placed on the emitting material.

This material is based upon work supported by the National Science Foundation under grant AST 84-15142. It was also supported in part by the National Aeronautics and Space Administration under grants NAG8-431 and NAG5-629.

REFERENCES

Bregmann, J. N., and Glassgold, A. E. 1982, *Ap. J.*, **263**, 564.
Cox, D. P. 1981, *Ap. J.*, **245**, 534.
———. 1983, in *Supernova Remnants and Their X-Ray Emission*, ed. J. Danziger and P. Gorenstein (Dordrecht: Reidel), p. 385.
———. 1986a, *Ap. J.*, **304**, 771.
———. 1986b, in preparation.
Cox, D. P., and Anderson, P. R. 1982, *Ap. J.*, **253**, 268.
Cox, D. P., and Franco, J. 1981, *Ap. J.*, **251**, 687.
Hamilton, A. J. S., Sarazin, C. L., and Chevalier, R. A. 1982, *Ap. J. Suppl.*, **51**, 115.
Long, K. L. 1983, in *Supernova Remnants and Their X-Ray Emission*, ed. J. Danziger and P. Gorenstein (Dordrecht: Reidel), 525.
McCammon, D., and Sanders, W. T. 1984, *Ap. J.*, **287**, 167 (McS).
McKee, C. F., and Ostriker, J. P. 1977, *Ap. J.*, **218**, 148 (MO).
Raymond, J. C., and Smith, B. W. 1977, *Ap. J. Suppl.*, **35**, 419.
———. 1979, private communication (update to Raymond and Smith 1977).

DONALD P. COX and DAN MCCAMMON: Department of Physics, University of Wisconsin, Madison, 1150 University Avenue, Madison, WI 53706